Nuclear Engineering and Technology 49 (2017) 1758–1771

Contents lists available at ScienceDirect

Nuclear Engineering and Technology

journal homepage: www.elsevier.com/locate/net

Original Article

Investigation on radiation shielding parameters of cerrobend alloys

Borhan Tellili [a, b], Youssef Elmahroug [a, *], Chedly Souga [c]

[a] Université de Tunis El Manar, Faculté des Sciences de Tunis, Département de physique, Unité de Recherche de Physique Nucléaire et des Hautes Energies, Campus Universitaire El-Manar, 2092 El Manar Tunis, Tunisia
[b] Université de Tunis El Manar, Institut Supérieur des Technologies Médicales de Tunis, Département de physique, 9 Rue Zouhair Essafi, 1006 Tunis, Tunisia
[c] Université de Carthage, École Polytechnique de Tunisie, B.P. 743, 2078, La Marsa, Tunisia

ARTICLE INFO

Article history:
Received 14 February 2016
Received in revised form
28 July 2017
Accepted 8 August 2017
Available online 2 November 2017

Keywords:
Cerrobend Alloys
Effective Atomic Number and Electron Density
Half Value Layer
Tenth Value Layer
Total Mass Attenuation Coefficients

ABSTRACT

In this study, to determine the most effective alloy for shielding against gamma-rays, the gamma-ray shielding parameters of six types of cerrobend alloys have been investigated. Gamma-ray interaction with the cerrobend alloys has been discussed mainly in terms of total mass attenuation coefficient (μ_t), half value layer (HVL), tenth value layer (TVL), effective atomic number (Z_{eff}), and effective electron density (N_{eff}). These parameters have been calculated by theoretical approach using the ParShield program in a photon energy range between 0.1 MeV and 100 GeV. The dependence of these parameters on the incident photon energy and chemical composition of the cerrobend alloys has been studied.

1. Introduction

With the increasing use of gamma-rays and x-rays in medicine, particularly in radiotherapy and medical imaging, various human organs and tissues will be exposed to x-rays and gamma-rays, in particular during radiotherapy treatment; this can cause many dangerous diseases, such as breast and skin cancer. Hence, to minimize the risk of damage to healthy tissue and potentially serious side-effects, it is necessary to restrict and control exposure of human beings to these types of radiation by using shields of proper dimensions and of an appropriate material. The choice of suitable shielding materials requires a thorough understanding of the absorption and interaction of x-rays and gamma-rays with matter. Knowledge of photon interaction parameters is therefore very useful for radiation protection engineers in the design and manufacture of gamma radiation shielding. The total mass attenuation coefficient (μ_t), the half value layer (HVL), the tenth value layer (TVL), the effective atomic number (Z_{eff}), and the effective electron density (N_{eff}) are the basic quantities used in calculations and the study of the penetration of x-rays and gamma-rays in to shielding materials and other materials.

The total mass attenuation coefficient (μ_t) is a measure of the probability of interactions that occur between incident photons and the thickness of the target material; it is measured in cm^2/g [10,11]. It is a fundamental parameter used in the calculation of many other photon interaction parameters such as absorbed dose, energy absorption, build-up factor, Kinetic Energy Released in Materials (KERMA), mean free path, HVL, equivalent and effective atomic numbers, electron density, molecular cross-section, atomic cross-section, and electronic cross-section, e.g., in designs of radiation shielding. The values of this coefficient are used in several fields such as radiotherapy, nuclear diagnostics, radiation protection, radiation dosimetry, radiation biophysics, etc. The mass attenuation coefficients of different materials have been determined in several works [1,2,5,7,8,12,13,15]. The magnitude of this coefficient depends on the incident photon energy, the material density, and the atomic number of elements. In the case of a composite material (compound and mixture), consisting of several elements in varying proportions, the total mass attenuation coefficient depends on another number called the "effective atomic number (Z_{eff})," which varies with the incident photon energy. Indeed, the partial interaction cross-section depends on the chemical composition of the material; a single, unique atomic number across the entire energy region, cannot describe the chemical properties of composite materials in an entire energy range, as is possible for pure elements.

* *Corresponding author.*
E-mail address: youssef_phy@hotmail.fr (Y. Elmahroug).

https://doi.org/10.1016/j.net.2017.08.020

The idea of this number is to assume that a compound or a mixture can be considered as a simple element characterized by the atomic number (Z_{eff}); however, this value is not constant, it varies with the incident photon energy. The notion and the theoretical expression of this parameter were suggested by Hine [9]. The effective atomic number is related to another important physical parameter called the effective electron density (N_{eff}), which is defined as the number of electrons per unit mass of the target material [1,2,5,7,8,12,15].

In the present work, some radiation shielding parameters such as the total mass attenuation coefficient (μ_t), the HVL, the TVL, the effective atomic number (Z_{eff}), and the effective electron density (N_{eff}) of six types of cerrobend alloys were investigated. The total mass attenuation coefficient, the effective atomic number, and the effective electron density were calculated using the ParShield program for a photon energy range of 0.1 MeV–100 GeV. The HVL and TVL were calculated using the values of μ_t. The ParShield program was written in C++; it runs on the Windows operating system [6]. It was developed to calculate the gamma and neutron shielding parameters for compounds or mixtures. ParShield can calculate the total mass attenuation coefficient, the effective atomic number, and the effective electron density for any compound or mixture, at energies from 1 keV to 100 GeV. It can also calculate the macroscopic effective removal cross-sections of fast neutrons for compounds or mixtures. The predictions of this program were tested and validated by comparing them with the experimental results and the results obtained using the programs WinXcom and MERCSF-N, for which good agreement was found [6]. A description of this program (the equations and the database used) is available in the Elmahroug's study [6].

The aim of this study is to make a comparison between these materials to determine what the materials are effective for gamma rays shielding. The present work will be of prime importance for radiation shield design in radiotherapy and medical imaging. The results of the present investigation may help in selecting appropriate shielding material and determining the optimum thickness of blocks; it will also help in calculating the absorbed dose. Indeed, cerrobend alloys are used in several areas, especially in radiation therapy applications [3,4,14,16–18]. They are often used as custom blocks to form a special open size that can fit the shape of a tumor to minimize the dose outside of the patient's treatment field [3,4,14,16–18]. The following are the major advantages of cerrobend alloys: (1) high density; (2) low melting temperature, but solid at room temperature; (3) easy molding and reuse; (4) ease of shaping; (5) low cost; and (6) consist of elements of high atomic number (Cd, In, Sn, Sb, Bi, and Pb). The chemical compositions of the six types of cerrobend alloys studied in this work were obtained from CS Alloys Company (2888 Colony Woods Drive Gastonia, NC 28054, USA) and have been listed in Table 1.

2. Theoretical method

2.1. Total mass attenuation coefficient

During its passage through a material medium, a photon undergoes several interactions such as photoelectric absorption, coherent scattering, incoherent scattering, and pair production. If a photon beam having an initial intensity (I_0) penetrates matter, it will be attenuated and its intensity decreases exponentially according to the following exponential law:

$$I = I_0 e^{-\left(\frac{\mu}{\rho}\right)\rho x} = I_0 e^{-\mu_t d} \quad (1)$$

This is called the Beer-Lambert law, where I is the transmitted intensity, μ is the linear attenuation coefficient in cm^{-1}, ρ is the material density in g/cm^3, x is the thickness of the absorbing medium, d is the mass per unit area (cm^2/g), and $\mu_t = \mu/\rho$ is the total mass attenuation coefficient (cm^2/g). For a chemical mixture composed of various elements and compounds, as in our case, the total mass attenuation coefficient of the mixture (μ_t) is given by the following "mixture rule":

$$\mu_t = \sum_i w_i (\mu_t)_i \quad (2)$$

where $(\mu_t)_i$ and w_i are, respectively, the total mass attenuation coefficient and the fractional weight of the i^{th} constituent in the mixture.

2.2. HVL and TVL

To correctly choose the optimum thickness of a material used for shielding purposes, it is necessary to have knowledge of the values of the HVL and the TVL. These two parameters are commonly used in shielding calculation, especially in radiotherapy and medical imaging. The HVL is the thickness of the shielding material required to reduce the incident beam intensity by one-half. The TVL could be defined in the same way: it is the thickness of the shielding material required to reduce the radiation intensity to one-tenth of its initial intensity. The HVL and TVL are expressed in units of distance (cm or mm). Like the attenuation coefficient, the values of HVL and TVL are dependent on the energy of the photon radiation and the type of material. HVL and TVL are inversely proportional to the linear attenuation coefficient (μ) and are related as follows:

$$HVL = \frac{0.693}{\mu} \quad (3)$$

The unit of (μ) is cm^{-1} and that of HVL is cm.

$$TVL = \frac{2.3026}{\mu} \quad (4)$$

2.3. Effective atomic number and effective electron density

The effective atomic number (Z_{eff}) is defined as the ratio of the total atomic effective cross-section to the total electronic effective cross-section:

$$Z_{eff} = \frac{\sigma_a}{\sigma_e} \quad (5)$$

Table 1
Chemical composition (%) of cerrobend alloys used in this work.

Element	Low 136 alloy ($\rho = 8.58$ g/cm^3)	Bend alloy ($\rho = 9.38$ g/cm^3)	Tru alloy ($\rho = 8.72$ g/cm^3)	Low 147 alloy ($\rho = 9.47$ g/cm^3)	Safe alloy ($\rho = 9.44$ g/cm^3)	Cast alloy ($\rho = 8.19$ g/cm^3)
Cd	–	10.0	–	9.6	8.5	–
In	21.0	–	–	4.0	–	–
Sn	12.0	13.3	42.0	12.8	11.3	–
Pb	22.6	26.67	–	25.6	37.7	60.0
Bi	49.0	50.0	58.0	48.0	42.5	40.0

Table 2
Total mass attenuation coefficient (μ_t) for cerrobend alloys used in this work.

Energy (MeV)	Total mass attenuation coefficient (μ_t; cm^2/g)					
	Low 136 alloy	Bend alloy	Tru alloy	Low 147 alloy	Safe alloy	Cast alloy
1.00E−01	4.40E+00	4.73E+00	4.03E+00	4.60E+00	4.85E+00	3.30E+00
1.50E−01	1.60E+00	1.72E+00	1.46E+00	1.67E+00	1.76E+00	1.20E+00
2.00E−01	8.01E−01	8.57E−01	7.36E−01	8.35E−01	8.78E−01	6.09E−01
3.00E−01	3.33E−01	3.53E−01	3.10E−01	3.46E−01	3.61E−01	2.65E−01
4.00E−01	1.99E−01	2.08E−01	1.87E−01	2.05E−01	2.12E−01	1.65E−01
5.00E−01	1.42E−01	1.48E−01	1.35E−01	1.45E−01	1.50E−01	1.23E−01
6.00E−01	1.12E−01	1.16E−01	1.08E−01	1.15E−01	1.17E−01	9.98E−02
8.00E−01	8.26E−02	8.44E−02	8.04E−02	8.37E−02	8.50E−02	7.61E−02
1.00E+00	6.75E−02	6.86E−02	6.62E−02	6.82E−02	6.89E−02	6.37E−02
1.50E+00	5.08E−02	5.12E−02	5.01E−02	5.10E−02	5.14E−02	4.90E−02
2.00E+00	4.48E−02	4.52E−02	4.43E−02	4.51E−02	4.53E−02	4.33E−02
3.00E+00	4.09E−02	4.13E−02	4.03E−02	4.11E−02	4.15E−02	3.92E−02
4.00E+00	4.02E−02	4.07E−02	3.96E−02	4.05E−02	4.09E−02	3.83E−02
5.00E+00	4.07E−02	4.13E−02	3.99E−02	4.10E−02	4.15E−02	3.86E−02
6.00E+00	4.16E−02	4.22E−02	4.08E−02	4.20E−02	4.25E−02	3.93E−02
7.00E+00	4.28E−02	4.35E−02	4.19E−02	4.32E−02	4.37E−02	4.02E−02
8.00E+00	4.40E−02	4.48E−02	4.31E−02	4.45E−02	4.51E−02	4.12E−02
9.00E+00	4.53E−02	4.61E−02	4.43E−02	4.58E−02	4.64E−02	4.24E−02
1.00E+01	4.66E−02	4.74E−02	4.55E−02	4.71E−02	4.78E−02	4.35E−02
1.10E+01	4.79E−02	4.88E−02	4.67E−02	4.84E−02	4.91E−02	4.46E−02
1.20E+01	4.91E−02	5.01E−02	4.79E−02	4.97E−02	5.04E−02	4.57E−02
1.30E+01	5.03E−02	5.13E−02	4.91E−02	5.09E−02	5.17E−02	4.68E−02
1.40E+01	5.15E−02	5.26E−02	5.02E−02	5.21E−02	5.30E−02	4.78E−02
1.50E+01	5.26E−02	5.37E−02	5.13E−02	5.33E−02	5.41E−02	4.88E−02
1.60E+01	5.37E−02	5.48E−02	5.23E−02	5.44E−02	5.53E−02	4.97E−02
1.80E+01	5.57E−02	5.69E−02	5.42E−02	5.64E−02	5.73E−02	5.15E−02
2.00E+01	5.75E−02	5.87E−02	5.60E−02	5.82E−02	5.92E−02	5.31E−02
2.20E+01	5.92E−02	6.05E−02	5.76E−02	6.00E−02	6.10E−02	5.46E−02
2.40E+01	6.08E−02	6.21E−02	5.91E−02	6.16E−02	6.27E−02	5.60E−02
2.60E+01	6.22E−02	6.36E−02	6.05E−02	6.31E−02	6.42E−02	5.73E−02
2.80E+01	6.36E−02	6.50E−02	6.18E−02	6.44E−02	6.56E−02	5.85E−02
3.00E+01	6.48E−02	6.63E−02	6.31E−02	6.57E−02	6.69E−02	5.96E−02
4.00E+01	7.01E−02	7.18E−02	6.82E−02	7.11E−02	7.24E−02	6.44E−02
5.00E+01	7.42E−02	7.59E−02	7.21E−02	7.52E−02	7.66E−02	6.80E−02
6.00E+01	7.74E−02	7.92E−02	7.52E−02	7.85E−02	7.99E−02	7.09E−02
8.00E+01	8.22E−02	8.41E−02	7.98E−02	8.33E−02	8.49E−02	7.52E−02
1.00E+02	8.56E−02	8.76E−02	8.31E−02	8.68E−02	8.84E−02	7.83E−02
1.50E+02	9.11E−02	9.33E−02	8.84E−02	9.24E−02	9.41E−02	8.34E−02
2.00E+02	9.44E−02	9.66E−02	9.17E−02	9.58E−02	9.76E−02	8.64E−02
3.00E+02	9.83E−02	1.01E−01	9.54E−02	9.97E−02	1.02E−01	9.00E−02
4.00E+02	1.01E−01	1.03E−01	9.76E−02	1.02E−01	1.04E−01	9.20E−02
5.00E+02	1.02E−01	1.04E−01	9.90E−02	1.03E−01	1.05E−01	9.34E−02
6.00E+02	1.03E−01	1.06E−01	1.00E−01	1.05E−01	1.07E−01	9.43E−02
8.00E+02	1.05E−01	1.07E−01	1.02E−01	1.06E−01	1.08E−01	9.57E−02
1.00E+03	1.05E−01	1.08E−01	1.02E−01	1.07E−01	1.09E−01	9.65E−02
1.50E+03	1.07E−01	1.09E−01	1.04E−01	1.08E−01	1.10E−01	9.77E−02
2.00E+03	1.07E−01	1.10E−01	1.04E−01	1.09E−01	1.11E−01	9.84E−02
3.00E+03	1.08E−01	1.11E−01	1.05E−01	1.10E−01	1.12E−01	9.91E−02
4.00E+03	1.09E−01	1.11E−01	1.06E−01	1.10E−01	1.12E−01	9.95E−02
5.00E+03	1.09E−01	1.12E−01	1.06E−01	1.11E−01	1.13E−01	9.98E−02
6.00E+03	1.09E−01	1.12E−01	1.06E−01	1.11E−01	1.13E−01	9.99E−02
8.00E+03	1.09E−01	1.12E−01	1.06E−01	1.11E−01	1.13E−01	1.00E−01
1.00E+04	1.10E−01	1.12E−01	1.06E−01	1.11E−01	1.13E−01	1.00E−01
1.50E+04	1.10E−01	1.12E−01	1.07E−01	1.11E−01	1.13E−01	1.01E−01
2.00E+04	1.10E−01	1.12E−01	1.07E−01	1.11E−01	1.14E−01	1.01E−01
3.00E+04	1.10E−01	1.13E−01	1.07E−01	1.12E−01	1.14E−01	1.01E−01
4.00E+04	1.10E−01	1.13E−01	1.07E−01	1.12E−01	1.14E−01	1.01E−01
5.00E+04	1.10E−01	1.13E−01	1.07E−01	1.12E−01	1.14E−01	1.01E−01
6.00E+04	1.10E−01	1.13E−01	1.07E−01	1.12E−01	1.14E−01	1.01E−01
8.00E+04	1.10E−01	1.13E−01	1.07E−01	1.12E−01	1.14E−01	1.01E−01
1.00E+05	1.10E−01	1.13E−01	1.07E−01	1.12E−01	1.14E−01	1.01E−01

The total atomic cross-section (σ_a) can be derived from the values of the total mass attenuation coefficients by the following relation:

$$\sigma_a = \frac{\mu_t}{N_A \sum_i \frac{w_i}{A_i}} \tag{6}$$

where N_A is Avogadro number and A_i is the molar mass of the i^{th} constituent in the mixture. Similarly, the total electronic cross-section (σ_e) is given by the following formula:

$$\sigma_e = \frac{1}{N_A} \sum_i \left(\sum_j \frac{f_j A_j}{Z_j} (\mu_t)_j \right) w_i \tag{7}$$

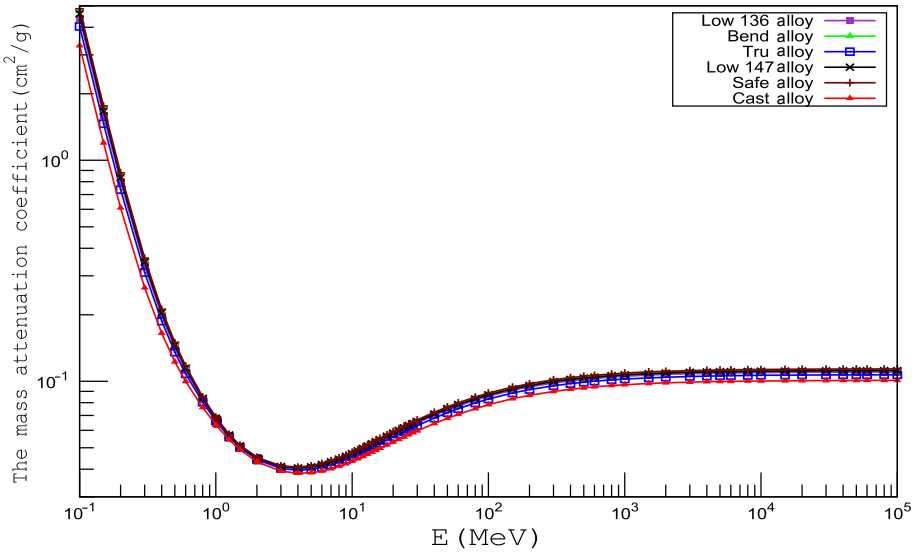

Fig. 1. The variation of total mass attenuation coefficients of cerrobend alloys with incident photon energies.

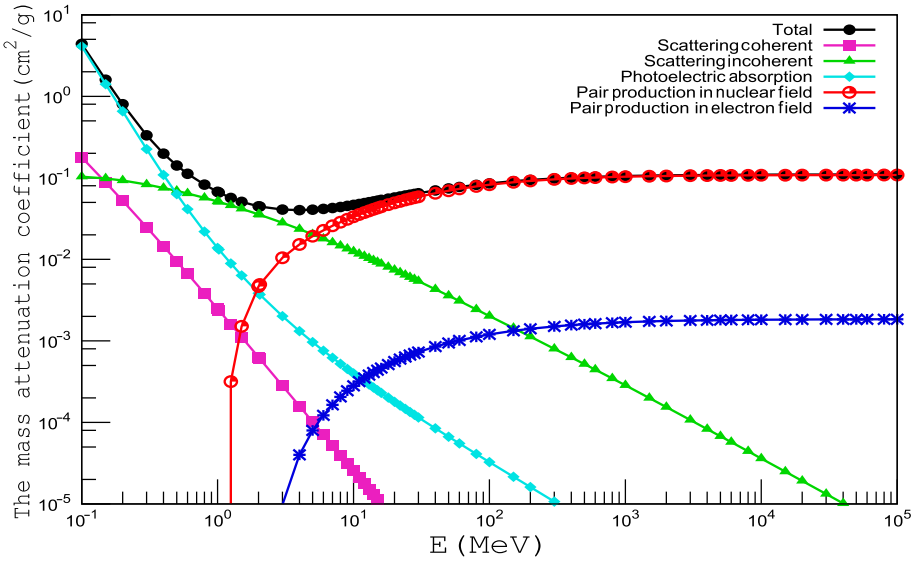

Fig. 2. The variation of total and partial mass attenuation coefficients with incident photon energies.

where $(\mu_t)_j$, f_j, and Z_j are, respectively, the total mass attenuation coefficient, the fractional abundance, and the atomic number of the j^{th} element in the i^{th} constituent.

Finally, the effective electron number or the density (N_{eff}; the electrons number per unit mass, electron/g) is closely related to Z_{eff} and can be found from the following equation:

$$N_{eff} = \frac{\mu_t}{\sigma_e} = \frac{Z_{eff} N_A}{\sum_i \frac{w_i}{A_i}} \tag{8}$$

3. Results and discussion

3.1. Total mass attenuation coefficient

Table 2 lists the obtained values of the total mass attenuation coefficient for all cerrobend alloys used in this study for the energy range of 0.1 MeV–100 GeV. In addition, the variations of the total mass attenuation coefficients (μ_t), with the incident photon energy for all alloys have been shown graphically in Fig. 1. It can be clearly seen in this figure that the total mass attenuation coefficients depend on the incident photon energy and the concentration of elements within alloys. It can also be clearly seen in this figure that the behaviors of μ_t with the incident photon energy for all the alloys considered in this work are almost identical. Maximum values of μ_t have been observed at low energies. However, low values of μ_t have been observed at intermediate energies. The dependence of the mass absorption coefficient on the chemical composition is large at the lower energy region and negligible at intermediate energies; furthermore, there is a significant variation in μ_t in the high energy region. The dependence of μ_t on the incident photon energy and the chemical composition can be attributed to domination of the different photon interaction processes with materials in different energy regions. The contributions of different photon interaction processes (photoelectric absorption, Compton scattering, and pair

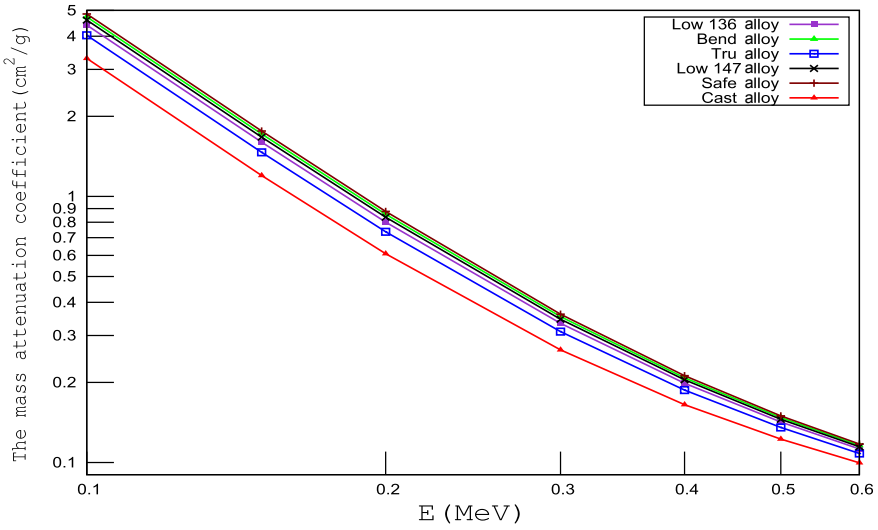

Fig. 3. The variation of total mass attenuation coefficients of cerrobend alloys with incident photon energies for the energy range of 0.1 MeV–0.6 MeV.

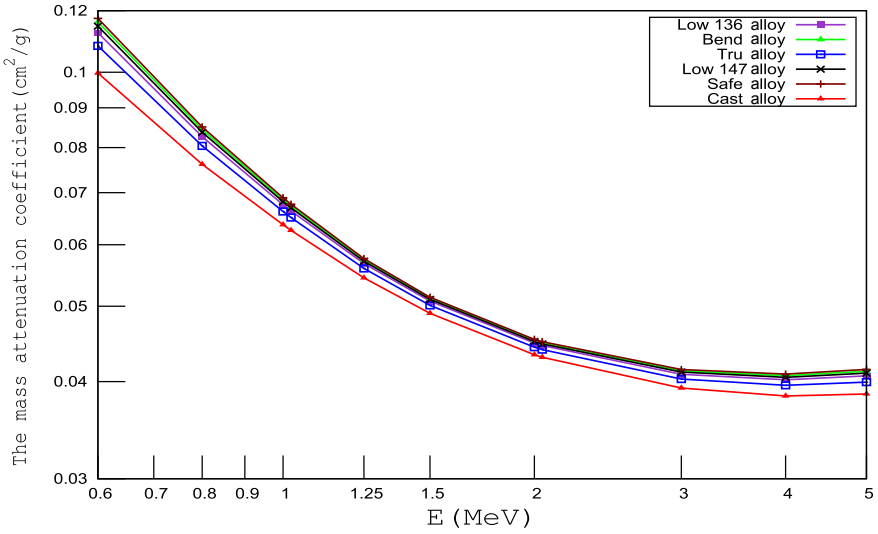

Fig. 4. The variation of total mass attenuation coefficients of cerrobend alloys with incident photon energies for the energy range of 0.6 MeV–5 MeV.

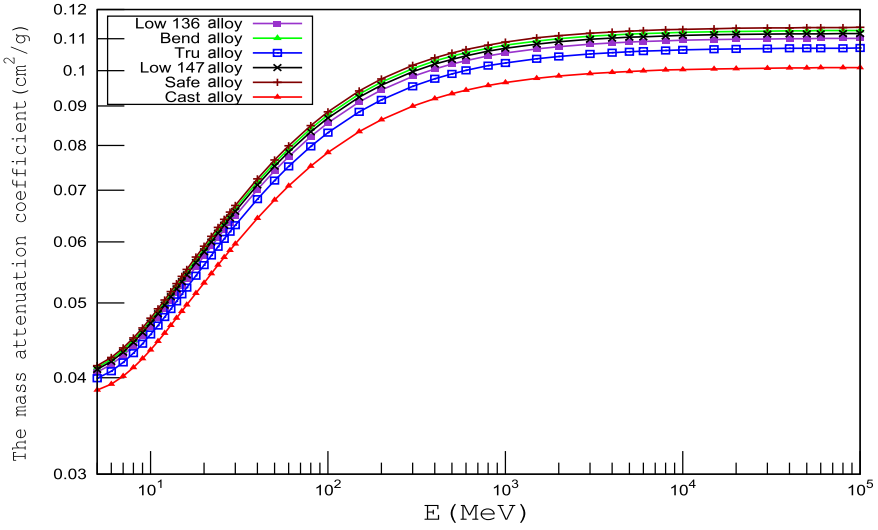

Fig. 5. The variation of total mass attenuation coefficients of cerrobend alloys with incident photon energies for the energy range of 5 MeV–100 GeV.

Table 3
HVL for cerrobend alloys used in this work.

Energy (MeV)	Half value layer (cm)					
	Low 136 alloy	Bend alloy	Tru alloy	Low 147 alloy	Safe alloy	Cast alloy
1.00E−01	1.84E−02	1.56E−02	1.97E−02	1.59E−02	1.51E−02	2.56E−02
1.50E−01	5.05E−02	4.30E−02	5.43E−02	4.38E−02	4.17E−02	7.06E−02
2.00E−01	1.01E−01	8.62E−02	1.08E−01	8.77E−02	8.36E−02	1.39E−01
3.00E−01	2.42E−01	2.09E−01	2.56E−01	2.12E−01	2.03E−01	3.19E−01
4.00E−01	4.07E−01	3.55E−01	4.25E−01	3.58E−01	3.47E−01	5.13E−01
5.00E−01	5.69E−01	5.00E−01	5.87E−01	5.04E−01	4.91E−01	6.91E−01
6.00E−01	7.19E−01	6.37E−01	7.35E−01	6.39E−01	6.26E−01	8.48E−01
8.00E−01	9.78E−01	8.75E−01	9.89E−01	8.75E−01	8.64E−01	1.11E+00
1.00E+00	1.20E+00	1.08E+00	1.20E+00	1.07E+00	1.07E+00	1.33E+00
1.50E+00	1.59E+00	1.44E+00	1.59E+00	1.43E+00	1.43E+00	1.73E+00
2.00E+00	1.80E+00	1.63E+00	1.79E+00	1.63E+00	1.62E+00	1.95E+00
3.00E+00	1.98E+00	1.79E+00	1.97E+00	1.78E+00	1.77E+00	2.16E+00
4.00E+00	2.01E+00	1.81E+00	2.01E+00	1.81E+00	1.80E+00	2.21E+00
5.00E+00	1.99E+00	1.79E+00	1.99E+00	1.79E+00	1.77E+00	2.19E+00
6.00E+00	1.94E+00	1.75E+00	1.95E+00	1.74E+00	1.73E+00	2.16E+00
7.00E+00	1.89E+00	1.70E+00	1.90E+00	1.70E+00	1.68E+00	2.10E+00
8.00E+00	1.84E+00	1.65E+00	1.85E+00	1.65E+00	1.63E+00	2.05E+00
9.00E+00	1.78E+00	1.60E+00	1.80E+00	1.60E+00	1.58E+00	2.00E+00
1.00E+01	1.73E+00	1.56E+00	1.75E+00	1.55E+00	1.54E+00	1.95E+00
1.10E+01	1.69E+00	1.51E+00	1.70E+00	1.51E+00	1.49E+00	1.90E+00
1.20E+01	1.64E+00	1.48E+00	1.66E+00	1.47E+00	1.46E+00	1.85E+00
1.30E+01	1.60E+00	1.44E+00	1.62E+00	1.44E+00	1.42E+00	1.81E+00
1.40E+01	1.57E+00	1.41E+00	1.58E+00	1.40E+00	1.39E+00	1.77E+00
1.50E+01	1.53E+00	1.38E+00	1.55E+00	1.37E+00	1.36E+00	1.73E+00
1.60E+01	1.50E+00	1.35E+00	1.52E+00	1.35E+00	1.33E+00	1.70E+00
1.80E+01	1.45E+00	1.30E+00	1.47E+00	1.30E+00	1.28E+00	1.64E+00
2.00E+01	1.40E+00	1.26E+00	1.42E+00	1.26E+00	1.24E+00	1.59E+00
2.20E+01	1.36E+00	1.22E+00	1.38E+00	1.22E+00	1.20E+00	1.55E+00
2.40E+01	1.33E+00	1.19E+00	1.34E+00	1.19E+00	1.17E+00	1.51E+00
2.60E+01	1.30E+00	1.16E+00	1.31E+00	1.16E+00	1.14E+00	1.48E+00
2.80E+01	1.27E+00	1.14E+00	1.29E+00	1.14E+00	1.12E+00	1.45E+00
3.00E+01	1.25E+00	1.11E+00	1.26E+00	1.11E+00	1.10E+00	1.42E+00
4.00E+01	1.15E+00	1.03E+00	1.17E+00	1.03E+00	1.01E+00	1.31E+00
5.00E+01	1.09E+00	9.73E−01	1.10E+00	9.74E−01	9.59E−01	1.24E+00
6.00E+01	1.04E+00	9.33E−01	1.06E+00	9.33E−01	9.19E−01	1.19E+00
8.00E+01	9.83E−01	8.78E−01	9.97E−01	8.79E−01	8.65E−01	1.12E+00
1.00E+02	9.44E−01	8.43E−01	9.57E−01	8.43E−01	8.30E−01	1.08E+00
1.50E+02	8.87E−01	7.92E−01	8.99E−01	7.93E−01	7.80E−01	1.01E+00
2.00E+02	8.56E−01	7.64E−01	8.67E−01	7.65E−01	7.53E−01	9.79E−01
3.00E+02	8.22E−01	7.34E−01	8.33E−01	7.35E−01	7.23E−01	9.41E−01
4.00E+02	8.04E−01	7.18E−01	8.15E−01	7.18E−01	7.07E−01	9.20E−01
5.00E+02	7.92E−01	7.08E−01	8.03E−01	7.08E−01	6.97E−01	9.06E−01
6.00E+02	7.84E−01	7.00E−01	7.94E−01	7.01E−01	6.90E−01	8.97E−01
8.00E+02	7.73E−01	6.91E−01	7.83E−01	6.91E−01	6.81E−01	8.84E−01
1.00E+03	7.66E−01	6.85E−01	7.77E−01	6.85E−01	6.74E−01	8.77E−01
1.50E+03	7.57E−01	6.76E−01	7.67E−01	6.77E−01	6.66E−01	8.66E−01
2.00E+03	7.52E−01	6.72E−01	7.62E−01	6.72E−01	6.62E−01	8.60E−01
3.00E+03	7.47E−01	6.67E−01	7.56E−01	6.67E−01	6.57E−01	8.54E−01
4.00E+03	7.44E−01	6.64E−01	7.54E−01	6.64E−01	6.55E−01	8.50E−01
5.00E+03	7.42E−01	6.63E−01	7.51E−01	6.63E−01	6.53E−01	8.48E−01
6.00E+03	7.40E−01	6.61E−01	7.50E−01	6.62E−01	6.52E−01	8.47E−01
8.00E+03	7.39E−01	6.60E−01	7.49E−01	6.60E−01	6.50E−01	8.44E−01
1.00E+04	7.38E−01	6.59E−01	7.47E−01	6.59E−01	6.49E−01	8.43E−01
1.50E+04	7.36E−01	6.58E−01	7.46E−01	6.58E−01	6.48E−01	8.42E−01
2.00E+04	7.36E−01	6.57E−01	7.45E−01	6.57E−01	6.47E−01	8.41E−01
3.00E+04	7.35E−01	6.57E−01	7.44E−01	6.57E−01	6.46E−01	8.40E−01
4.00E+04	7.34E−01	6.56E−01	7.44E−01	6.56E−01	6.46E−01	8.39E−01
5.00E+04	7.34E−01	6.56E−01	7.44E−01	6.56E−01	6.46E−01	8.39E−01
6.00E+04	7.34E−01	6.55E−01	7.44E−01	6.56E−01	6.46E−01	8.38E−01
8.00E+04	7.34E−01	6.55E−01	7.44E−01	6.56E−01	6.46E−01	8.38E−01
1.00E+05	7.34E−01	6.55E−01	7.43E−01	6.56E−01	6.45E−01	8.38E−01

HVL, half value layer.

production in the nuclear and electronic fields) are shown graphically in Fig. 2. This figure shows that the variation of the total mass attenuation coefficients with the incident photon energy and the dependence of these coefficients on the chemical content can be explained by the dominance of the partial photon interaction processes with matter (photoelectric absorption, Compton scattering, and pair production in the nuclear and electronic fields) in the following three energy regions: low ($E < 0.6$ MeV), intermediate (0.6 MeV $< E <$ 5 MeV), and high photon energy ($E > 5$ MeV).

In the low incident photon energy region ($E < 0.6$ MeV), the total mass attenuation coefficient (μ_t) decreases rapidly with the increase of the incident photon energy for all the selected alloys. Fig. 3 shows that the difference between the values of the mass attenuation coefficients of the materials in this region is very large

Table 4
TVL for cerrobend alloys used in this work.

Energy (MeV)	Tenth value layer (cm)					
	Low 136 alloy	Bend alloy	Tru alloy	Low 147 alloy	Safe alloy	Cast alloy
1.00E−01	6.10E−02	5.19E−02	6.55E−02	5.29E−02	5.03E−02	8.51E−02
1.50E−01	1.68E−01	1.43E−01	1.80E−01	1.46E−01	1.39E−01	2.35E−01
2.00E−01	3.35E−01	2.86E−01	3.59E−01	2.91E−01	2.78E−01	4.62E−01
3.00E−01	8.05E−01	6.94E−01	8.51E−01	7.04E−01	6.76E−01	1.06E+00
4.00E−01	1.35E+00	1.18E+00	1.41E+00	1.19E+00	1.15E+00	1.70E+00
5.00E−01	1.89E+00	1.66E+00	1.95E+00	1.67E+00	1.63E+00	2.29E+00
6.00E−01	2.39E+00	2.12E+00	2.44E+00	2.12E+00	2.08E+00	2.82E+00
8.00E−01	3.25E+00	2.91E+00	3.29E+00	2.91E+00	2.87E+00	3.69E+00
1.00E+00	3.97E+00	3.58E+00	3.99E+00	3.57E+00	3.54E+00	4.41E+00
1.50E+00	5.29E+00	4.79E+00	5.27E+00	4.77E+00	4.75E+00	5.74E+00
2.00E+00	5.99E+00	5.43E+00	5.96E+00	5.40E+00	5.38E+00	6.49E+00
3.00E+00	6.56E+00	5.94E+00	6.55E+00	5.91E+00	5.88E+00	7.16E+00
4.00E+00	6.67E+00	6.03E+00	6.68E+00	6.00E+00	5.96E+00	7.33E+00
5.00E+00	6.60E+00	5.95E+00	6.61E+00	5.93E+00	5.88E+00	7.29E+00
6.00E+00	6.45E+00	5.81E+00	6.47E+00	5.79E+00	5.74E+00	7.16E+00
7.00E+00	6.28E+00	5.65E+00	6.31E+00	5.63E+00	5.58E+00	6.99E+00
8.00E+00	6.10E+00	5.48E+00	6.13E+00	5.47E+00	5.42E+00	6.81E+00
9.00E+00	5.92E+00	5.32E+00	5.96E+00	5.31E+00	5.26E+00	6.64E+00
1.00E+01	5.76E+00	5.17E+00	5.80E+00	5.17E+00	5.11E+00	6.47E+00
1.10E+01	5.61E+00	5.03E+00	5.65E+00	5.02E+00	4.97E+00	6.30E+00
1.20E+01	5.46E+00	4.90E+00	5.51E+00	4.90E+00	4.84E+00	6.15E+00
1.30E+01	5.33E+00	4.78E+00	5.38E+00	4.77E+00	4.72E+00	6.01E+00
1.40E+01	5.21E+00	4.67E+00	5.26E+00	4.67E+00	4.61E+00	5.88E+00
1.50E+01	5.10E+00	4.57E+00	5.15E+00	4.57E+00	4.51E+00	5.76E+00
1.60E+01	5.00E+00	4.48E+00	5.05E+00	4.47E+00	4.41E+00	5.65E+00
1.80E+01	4.82E+00	4.32E+00	4.87E+00	4.31E+00	4.25E+00	5.46E+00
2.00E+01	4.67E+00	4.18E+00	4.72E+00	4.18E+00	4.12E+00	5.30E+00
2.20E+01	4.53E+00	4.06E+00	4.58E+00	4.06E+00	4.00E+00	5.15E+00
2.40E+01	4.42E+00	3.95E+00	4.47E+00	3.95E+00	3.89E+00	5.02E+00
2.60E+01	4.31E+00	3.86E+00	4.36E+00	3.86E+00	3.80E+00	4.91E+00
2.80E+01	4.22E+00	3.78E+00	4.27E+00	3.77E+00	3.72E+00	4.80E+00
3.00E+01	4.14E+00	3.70E+00	4.19E+00	3.70E+00	3.65E+00	4.71E+00
4.00E+01	3.83E+00	3.42E+00	3.88E+00	3.42E+00	3.37E+00	4.37E+00
5.00E+01	3.62E+00	3.23E+00	3.67E+00	3.23E+00	3.18E+00	4.13E+00
6.00E+01	3.47E+00	3.10E+00	3.51E+00	3.10E+00	3.05E+00	3.96E+00
8.00E+01	3.27E+00	2.92E+00	3.31E+00	2.92E+00	2.87E+00	3.74E+00
1.00E+02	3.14E+00	2.80E+00	3.18E+00	2.80E+00	2.76E+00	3.59E+00
1.50E+02	2.95E+00	2.63E+00	2.99E+00	2.63E+00	2.59E+00	3.37E+00
2.00E+02	2.84E+00	2.54E+00	2.88E+00	2.54E+00	2.50E+00	3.25E+00
3.00E+02	2.73E+00	2.44E+00	2.77E+00	2.44E+00	2.40E+00	3.12E+00
4.00E+02	2.67E+00	2.38E+00	2.71E+00	2.38E+00	2.35E+00	3.05E+00
5.00E+02	2.63E+00	2.35E+00	2.67E+00	2.35E+00	2.31E+00	3.01E+00
6.00E+02	2.61E+00	2.33E+00	2.64E+00	2.33E+00	2.29E+00	2.98E+00
8.00E+02	2.57E+00	2.30E+00	2.60E+00	2.29E+00	2.26E+00	2.94E+00
1.00E+03	2.55E+00	2.27E+00	2.58E+00	2.28E+00	2.24E+00	2.91E+00
1.50E+03	2.51E+00	2.25E+00	2.55E+00	2.25E+00	2.21E+00	2.88E+00
2.00E+03	2.50E+00	2.23E+00	2.53E+00	2.23E+00	2.20E+00	2.86E+00
3.00E+03	2.48E+00	2.21E+00	2.51E+00	2.22E+00	2.18E+00	2.84E+00
4.00E+03	2.47E+00	2.21E+00	2.50E+00	2.21E+00	2.17E+00	2.82E+00
5.00E+03	2.46E+00	2.20E+00	2.50E+00	2.20E+00	2.17E+00	2.82E+00
6.00E+03	2.46E+00	2.20E+00	2.49E+00	2.20E+00	2.16E+00	2.81E+00
8.00E+03	2.46E+00	2.19E+00	2.49E+00	2.19E+00	2.16E+00	2.80E+00
1.00E+04	2.45E+00	2.19E+00	2.48E+00	2.19E+00	2.16E+00	2.80E+00
1.50E+04	2.45E+00	2.19E+00	2.48E+00	2.19E+00	2.15E+00	2.80E+00
2.00E+04	2.44E+00	2.18E+00	2.48E+00	2.18E+00	2.15E+00	2.79E+00
3.00E+04	2.44E+00	2.18E+00	2.47E+00	2.18E+00	2.15E+00	2.79E+00
4.00E+04	2.44E+00	2.18E+00	2.47E+00	2.18E+00	2.15E+00	2.79E+00
5.00E+04	2.44E+00	2.18E+00	2.47E+00	2.18E+00	2.15E+00	2.79E+00
6.00E+04	2.44E+00	2.18E+00	2.47E+00	2.18E+00	2.15E+00	2.79E+00
8.00E+04	2.44E+00	2.18E+00	2.47E+00	2.18E+00	2.15E+00	2.79E+00
1.00E+05	2.44E+00	2.18E+00	2.47E+00	2.18E+00	2.14E+00	2.79E+00

TVL, tenth value layer.

compared with that of other regions. The strong dependence of μ_t on the incident photon energy and the chemical composition in this energy region can be explained based on the dominance of the photoelectric absorption at low energy, as shown in Fig. 2. It can be seen from this figure that in the low photon energy region, the photoelectric absorption is the dominant process; the contribution of other processes is negligible. Also, we can see that the partial mass attenuation coefficients of the photoelectric absorption decrease rapidly with increases in the incident photon energy. The rapid decrease in the attenuation coefficients for all the selected alloys in this region is due to the fact that the cross-section of the photoelectric absorption is inversely proportional to the incident photon energy, as $E^{3.5}$ [10,11]. On the other hand, the significant difference in the values of μ_t in the low energy region can also be

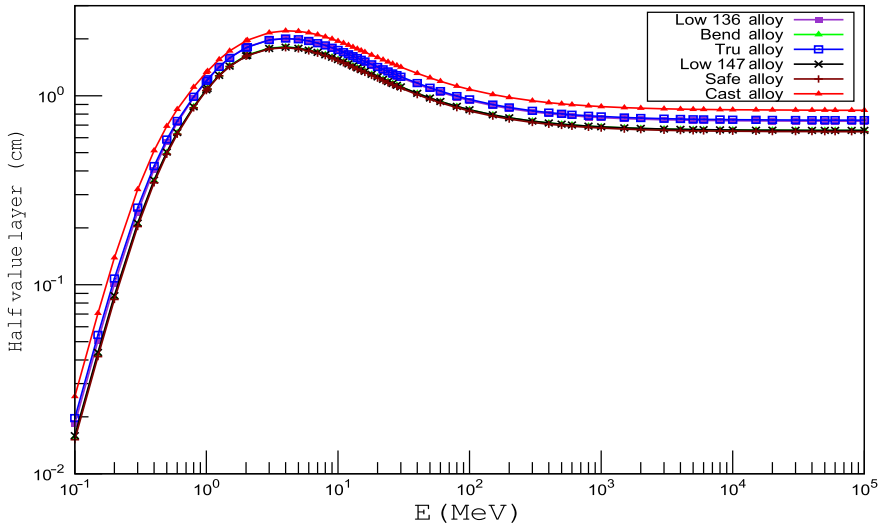

Fig. 6. The variation of half value layer of cerrobend alloys with incident photon energies.

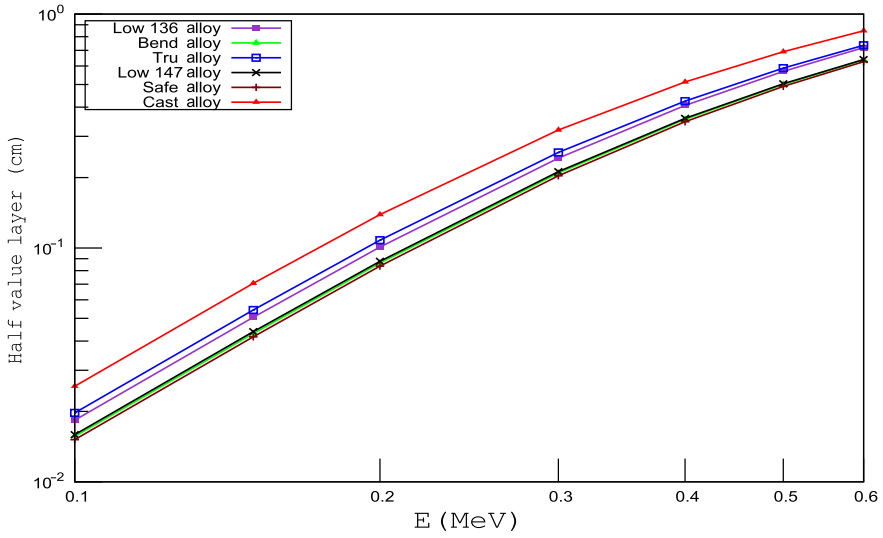

Fig. 7. The variation of half value layer of cerrobend alloys with incident photon energies for the energy range of 0.1 MeV–0.6 MeV.

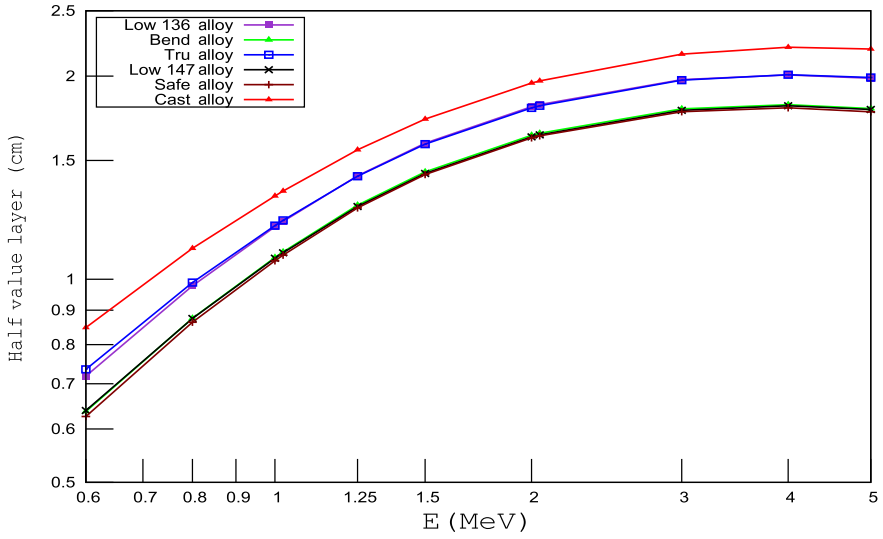

Fig. 8. The variation of half value layer of cerrobend alloys with incident photon energies for the energy range of 0.6 MeV–5 MeV.

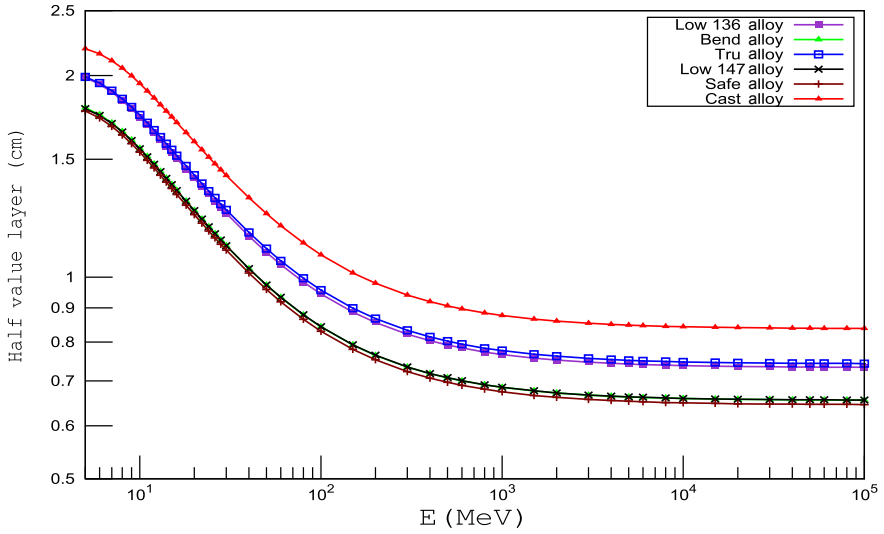

Fig. 9. The variation of half value layer of cerrobend alloys with incident photon energies for the energy range of 5 MeV–100 GeV.

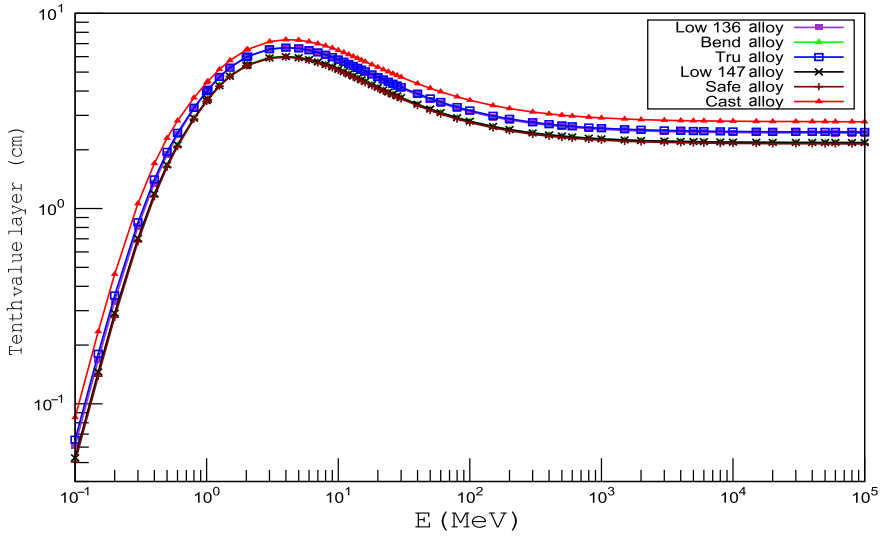

Fig. 10. The variation of tenth value layer of cerrobend alloys with incident photon energies.

attributed to the dominance of the photoelectric absorption because the photoelectric cross-section is strongly dependent on the atomic numbers of the constituent elements; it is proportional to the atomic number as Z^4 [10,11].

At intermediate incident photon energies, the mass attenuation coefficient decreases slowly with the increase of the incident photon energy and becomes almost constant as the incident photon energy approaches 3 MeV (Fig. 4). Furthermore, the difference between the values of μ_t becomes almost negligible compared with that observed in the low energy region; almost identical values have been observed for different alloys. This signifies that the chemical composition of the selected alloys plays a less significant role in the intermediate energy region. Fig. 2 shows that in this energy region, Compton scattering (especially incoherent scattering) becomes the main type of photon interaction; the partial mass attenuation coefficient decreases slowly with the increase of incident photon energy. The variation of this coefficient is due to the fact that the cross-section of the Compton scattering process is inversely proportional to the incident photon energy (E^{-1}) [10,11]. Therefore, the slow decrease in the values of μ_t at intermediate energy is mostly due to the contribution of the partial mass attenuation coefficient of the Compton scattering process; this also explains why lower values of the mass attenuation coefficients of all the alloys were obtained in this energy region (the minimum values of μ_t for all selected alloys have been observed at 5 MeV). On the other hand, the small difference observed between the values of μ_t of the six alloys in this energy region is due to the linear Z-dependence of the cross-section of the Compton scattering [10,11].

In the high energy region (5 MeV < E), the μ_t values increase gradually with the increase of the incident photon energy and become almost constant when the incident photon energy approaches 1 GeV (Fig. 5). Moreover, the variation in μ_t with chemical composition again becomes important, but it is less than the variation observed in low incident photon energy region (Fig. 5). These behaviors may result dominance of the pair-production process in the high energy region. Fig. 2 shows that the pair-production processes in the nuclear and electron fields become the dominant photon absorption processes after certain thresholds are exceeded (1.022 MeV and 2.044 MeV for pair-production in the nuclear and electron fields, respectively). It is also observed from this figure that

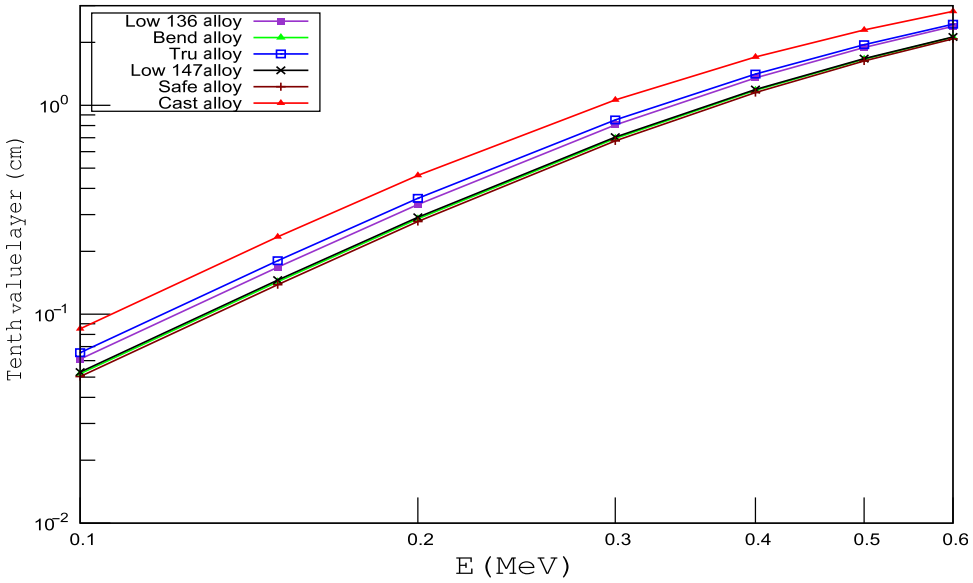

Fig. 11. The variation of tenth value layer of cerrobend alloys with incident photon energies for the energy range of 0.1 MeV–0.6 MeV.

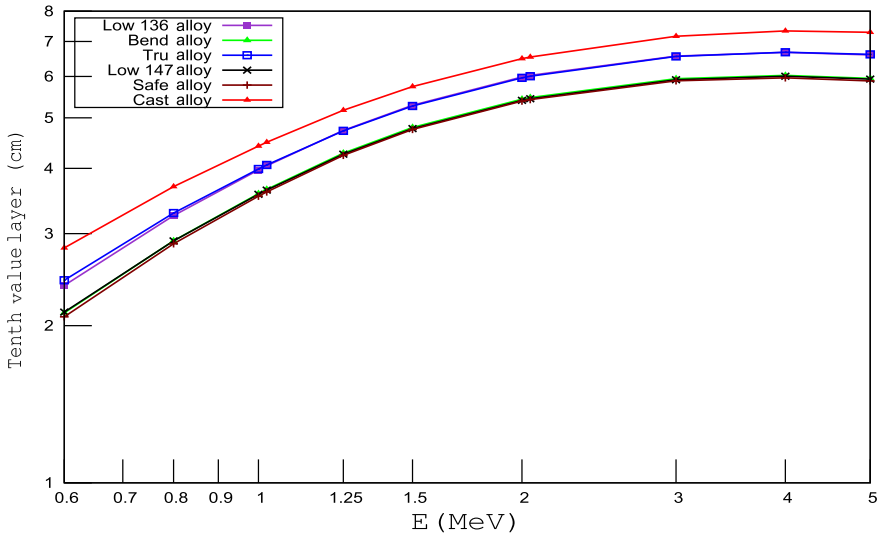

Fig. 12. The variation of tenth value layer of cerrobend alloys with incident photon energies for the energy range of 0.6 MeV–5 MeV.

the partial mass attenuation coefficients of pair-production in the nuclear and electron fields start, respectively, from 1.022 MeV and 2.044 MeV, and thereafter increase with the increase of the incident photon energy and become almost constant when the incident photon energy approaches 100 MeV. This also shows that the variation of the total mass attenuation coefficients in the high energy region is mostly due to the contribution of the partial mass attenuation coefficients of the pair-production processes. On the other hand, the variation of μ_t with the chemical composition can be explained based on Z-dependence of cross-section of pair production, which is proportional to Z^2 [10,11].

Finally, it can be seen from Figs. 3–5 and Table 2 that the alloy called the "Safe alloy" has the highest value of mass attenuation coefficient, whereas the alloy called the "Cast alloy" has the lowest value of mass attenuation coefficient. Although the alloys are composed of Cd, In, Sn, Sb, Pb, and Bi, the main influence on the total mass attenuation coefficient in this work is the amount of Pb and Bi in the alloys; alloys with Pb and Bi have higher values of total mass attenuation coefficients in comparison with those of the other alloys. The large amounts of Pb (37.7%) and Bi (42.5%) in the chemical composition of the Safe alloy in comparison with the case of the other alloys explain the greater value of μ_t for these alloys. On the other hand, the Cast alloy contains only Sn (60%) and Bi (40%), and hence has a lower total mass attenuation coefficient. Also, it can be seen from Table 2 that the values of the total mass attenuation coefficients of the Bend alloy and the Low 147 alloy are very close to that of the Safe alloy. This may be due to the concentration of Pb and Bi in these alloys, which is very close to that of the Safe alloy.

3.2. HVL and TVL

The HVL and TVL for all the selected cerrobend alloys were determined from Eqs. 3 and 4, respectively, and are given in Tables 3 and 4. The variations of the HVL and TVL with the incident photon energy are graphically shown in Figs. 6–13. From these

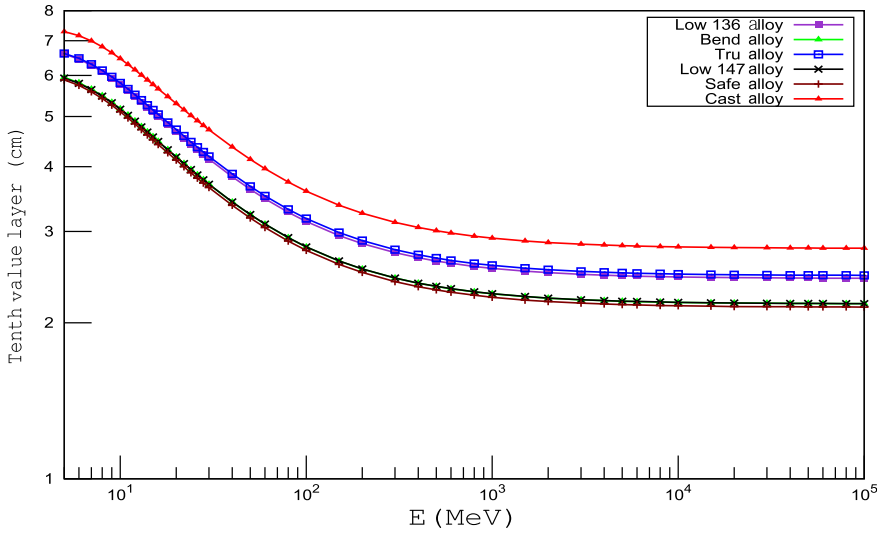

Fig. 13. The variation of tenth value layer of cerrobend alloys with incident photon energies for the energy range of 5 MeV–100 GeV.

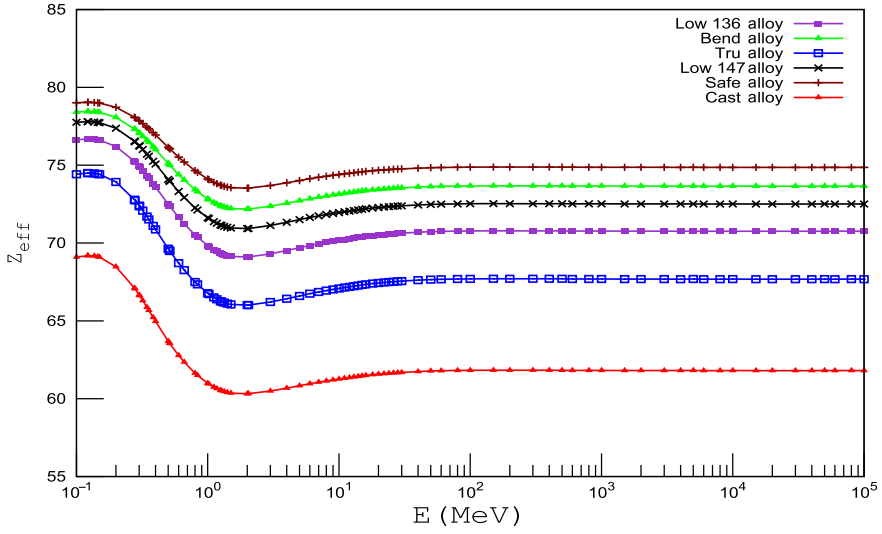

Fig. 14. The variation of the effective atomic number of cerrobend alloys with incident photon energies.

figures, it can be observed that initially, HVL and TVL have minimum values, which increase rapidly with the increase of the incident photon energy up to 4 MeV. Then, with further increase of the incident photon energy, the HVL and TVL values decrease slowly and become almost constant beyond 1 GeV. Like the variation of the value of μ_t, the variations of HVL and TVL can be explained by the dominance of different processes of photon interaction on different energy regions. On the other hand, it can be seen that the Cast alloy, the Tru alloy, and the Low 136 alloy have lowest values of HVL and TVL. This might be the result of the higher values of attenuation coefficient and the densities of these alloys.

3.3. Effective atomic number and effective electron density

Using the ParShield program, the values of Z_{eff} and N_{eff} of the six cerrobend alloys considered in this work have been determined at photon energies in the range of 1 keV–10 MeV. The ParShield program uses Eqs. 5 and 8 to calculate Z_{eff} and N_{eff}. The variations of the Z_{eff} values versus the incident photon energy for all the selected cerrobend alloys are presented in Fig. 14, and are tabulated in Table 5. It can be clearly seen in Fig. 14 and Table 5 that the effective electron number Z_{eff} is not a constant, but varies with the photon energy, as mentioned by Hine [9]. Moreover, the variations of Z_{eff} with the photon energy for all the alloys considered in this work are approximately identical. Initially, Z_{eff} decreased rapidly with the increase of the incident photon energy and reached a minimum at 2 MeV. After that, the value increased slowly and became constant. Also, it is seen from the Fig. 14 that Z_{eff} depends on the chemical composition of the alloys. As in the case with μ_t, the highest values of Z_{eff} have been observed for alloys that have higher amounts of Pb and Bi. The Safe alloy has the highest value of Z_{eff}, whereas the lowest value of Z_{eff} has been observed for the Cast alloy. As in the case of the variation of μ_t, the behaviors of Z_{eff} can be explained by the predominance of different processes of photon interaction in different energy regions.

The variations of the N_{eff} values with incident photon energy for all the selected cerrobend alloys are given in Table 6 and shown graphically in Fig. 15. It can be seen in this figure that N_{eff} varies with the photon energy. It is also clear that the variations of N_{eff} with the photon energy for all the selected alloys are similar to that

Table 5
Effective atomic number (Z_{eff}) for cerrobend alloys used in this work.

Energy (MeV)	Effective atomic number (Z_{eff})					
	Low 136 alloy	Bend alloy	Tru alloy	Low 147 alloy	Safe alloy	Cast alloy
1.00E−01	76.633	78.413	74.421	77.754	79.008	69.100
1.50E−01	76.612	78.393	74.414	77.732	78.991	69.092
2.00E−01	76.201	78.076	73.924	77.374	78.721	68.479
3.00E−01	74.920	77.076	72.402	76.253	77.862	66.667
4.00E−01	73.595	76.013	70.871	75.076	76.940	64.974
5.00E−01	72.494	75.110	69.638	74.085	76.148	63.696
6.00E−01	71.651	74.400	68.710	73.312	75.520	62.781
8.00E−01	70.518	73.427	67.496	72.263	74.652	61.638
1.00E+00	69.839	72.832	66.781	71.627	74.116	60.992
1.50E+00	69.141	72.211	66.058	70.967	73.555	60.360
2.00E+00	69.100	72.175	66.012	70.929	73.522	60.320
3.00E+00	69.307	72.362	66.213	71.128	73.693	60.494
4.00E+00	69.522	72.558	66.425	71.335	73.871	60.679
5.00E+00	69.697	72.715	66.600	71.503	74.014	60.832
6.00E+00	69.842	72.846	66.746	71.642	74.133	60.962
7.00E+00	69.953	72.945	66.858	71.748	74.222	61.061
8.00E+00	70.042	73.024	66.947	71.832	74.293	61.140
9.00E+00	70.115	73.089	67.022	71.902	74.352	61.208
1.00E+01	70.177	73.143	67.083	71.960	74.401	61.262
1.10E+01	70.230	73.191	67.138	72.011	74.444	61.312
1.20E+01	70.276	73.232	67.185	72.055	74.481	61.354
1.30E+01	70.320	73.270	67.230	72.096	74.516	61.395
1.40E+01	70.361	73.306	67.270	72.135	74.548	61.432
1.50E+01	70.397	73.338	67.307	72.169	74.577	61.466
1.60E+01	70.430	73.368	67.343	72.200	74.603	61.498
1.80E+01	70.481	73.412	67.396	72.248	74.643	61.546
2.00E+01	70.519	73.445	67.434	72.284	74.673	61.581
2.20E+01	70.549	73.472	67.465	72.312	74.697	61.610
2.40E+01	70.577	73.495	67.493	72.337	74.718	61.635
2.60E+01	70.598	73.514	67.517	72.358	74.735	61.657
2.80E+01	70.618	73.532	67.537	72.376	74.751	61.676
3.00E+01	70.634	73.546	67.554	72.392	74.763	61.691
4.00E+01	70.692	73.596	67.613	72.446	74.809	61.745
5.00E+01	70.726	73.627	67.651	72.479	74.836	61.781
6.00E+01	70.747	73.644	67.669	72.497	74.851	61.797
8.00E+01	70.766	73.662	67.693	72.516	74.868	61.819
1.00E+02	70.775	73.669	67.699	72.524	74.874	61.824
1.50E+02	70.781	73.676	67.707	72.531	74.880	61.832
2.00E+02	70.781	73.673	67.705	72.529	74.878	61.830
3.00E+02	70.779	73.673	67.702	72.529	74.878	61.828
4.00E+02	70.780	73.674	67.706	72.529	74.878	61.831
5.00E+02	70.776	73.671	67.701	72.526	74.875	61.826
6.00E+02	70.773	73.666	67.693	72.521	74.871	61.819
8.00E+02	70.771	73.664	67.692	72.519	74.869	61.818
1.00E+03	70.769	73.664	67.691	72.519	74.869	61.818
1.50E+03	70.764	73.660	67.685	72.514	74.866	61.812
2.00E+03	70.762	73.658	67.684	72.512	74.864	61.811
3.00E+03	70.764	73.659	67.685	72.514	74.865	61.812
4.00E+03	70.759	73.656	67.680	72.510	74.862	61.807
5.00E+03	70.764	73.660	67.688	72.515	74.866	61.815
6.00E+03	70.758	73.654	67.676	72.508	74.860	61.804
8.00E+03	70.757	73.653	67.678	72.507	74.859	61.805
1.00E+04	70.758	73.656	67.682	72.510	74.862	61.809
1.50E+04	70.756	73.653	67.677	72.507	74.859	61.804
2.00E+04	70.755	73.653	67.674	72.507	74.859	61.802
3.00E+04	70.757	73.654	67.679	72.508	74.860	61.806
4.00E+04	70.754	73.652	67.674	72.506	74.859	61.801
5.00E+04	70.758	73.656	67.681	72.510	74.861	61.808
6.00E+04	70.754	73.652	67.676	72.505	74.858	61.803
8.00E+04	70.760	73.657	67.683	72.511	74.863	61.810
1.00E+05	70.756	73.653	67.678	72.507	74.859	61.805

of Z_{eff}; this is normal because these two parameters are related through Eq. 8.

4. Conclusions

In this study, using the ParShield program, the values of total mass attenuation coefficient (μ_t), HVL, TVL, effective atomic number (Z_{eff}), and effective electron density (N_{eff}) for six cerrobend alloys were calculated in the energy region of 0.1 MeV–100 GeV. It can be concluded from the results obtained in this work that these parameters depend on the incident photon energy and the chemical composition of the alloys.

Because of the dominance of the photoelectric absorption process, the dependence of these parameters on both the incident photon energy and the chemical composition is remarkable in the low incident photon energy region. The compositional effects and

Table 6
Effective electron density (N_{eff}) for cerrobend alloys used in this work.

Energy (MeV)	Effective electron density (N_{eff}; electron/g)					
	Low 136 alloy	Bend alloy	Tru alloy	Low 147 alloy	Safe alloy	Cast alloy
1.00E−01	2.769E+23	2.688E+23	2.829E+23	2.722E+23	2.646E+23	2.900E+23
1.50E−01	2.768E+23	2.687E+23	2.829E+23	2.721E+23	2.645E+23	2.899E+23
2.00E−01	2.753E+23	2.676E+23	2.811E+23	2.709E+23	2.636E+23	2.874E+23
3.00E−01	2.707E+23	2.642E+23	2.753E+23	2.669E+23	2.608E+23	2.798E+23
4.00E−01	2.659E+23	2.605E+23	2.695E+23	2.628E+23	2.577E+23	2.727E+23
5.00E−01	2.619E+23	2.574E+23	2.648E+23	2.593E+23	2.550E+23	2.673E+23
6.00E−01	2.589E+23	2.550E+23	2.612E+23	2.566E+23	2.529E+23	2.635E+23
8.00E−01	2.548E+23	2.517E+23	2.566E+23	2.530E+23	2.500E+23	2.587E+23
1.00E+00	2.523E+23	2.496E+23	2.539E+23	2.507E+23	2.482E+23	2.560E+23
1.50E+00	2.498E+23	2.475E+23	2.512E+23	2.484E+23	2.463E+23	2.533E+23
2.00E+00	2.496E+23	2.474E+23	2.510E+23	2.483E+23	2.462E+23	2.531E+23
3.00E+00	2.504E+23	2.480E+23	2.517E+23	2.490E+23	2.468E+23	2.539E+23
4.00E+00	2.512E+23	2.487E+23	2.526E+23	2.497E+23	2.474E+23	2.546E+23
5.00E+00	2.518E+23	2.492E+23	2.532E+23	2.503E+23	2.479E+23	2.553E+23
6.00E+00	2.523E+23	2.497E+23	2.538E+23	2.508E+23	2.483E+23	2.558E+23
7.00E+00	2.527E+23	2.500E+23	2.542E+23	2.512E+23	2.486E+23	2.562E+23
8.00E+00	2.531E+23	2.503E+23	2.545E+23	2.515E+23	2.488E+23	2.566E+23
9.00E+00	2.533E+23	2.505E+23	2.548E+23	2.517E+23	2.490E+23	2.569E+23
1.00E+01	2.535E+23	2.507E+23	2.551E+23	2.519E+23	2.492E+23	2.571E+23
1.10E+01	2.537E+23	2.509E+23	2.553E+23	2.521E+23	2.493E+23	2.573E+23
1.20E+01	2.539E+23	2.510E+23	2.554E+23	2.522E+23	2.494E+23	2.575E+23
1.30E+01	2.541E+23	2.511E+23	2.556E+23	2.524E+23	2.496E+23	2.576E+23
1.40E+01	2.542E+23	2.513E+23	2.558E+23	2.525E+23	2.497E+23	2.578E+23
1.50E+01	2.543E+23	2.514E+23	2.559E+23	2.526E+23	2.498E+23	2.579E+23
1.60E+01	2.545E+23	2.515E+23	2.560E+23	2.527E+23	2.498E+23	2.581E+23
1.80E+01	2.546E+23	2.516E+23	2.562E+23	2.529E+23	2.500E+23	2.583E+23
2.00E+01	2.548E+23	2.517E+23	2.564E+23	2.530E+23	2.501E+23	2.584E+23
2.20E+01	2.549E+23	2.518E+23	2.565E+23	2.531E+23	2.502E+23	2.585E+23
2.40E+01	2.550E+23	2.519E+23	2.566E+23	2.532E+23	2.502E+23	2.587E+23
2.60E+01	2.551E+23	2.520E+23	2.567E+23	2.533E+23	2.503E+23	2.587E+23
2.80E+01	2.551E+23	2.520E+23	2.568E+23	2.534E+23	2.503E+23	2.588E+23
3.00E+01	2.552E+23	2.521E+23	2.568E+23	2.534E+23	2.504E+23	2.589E+23
4.00E+01	2.554E+23	2.522E+23	2.571E+23	2.536E+23	2.505E+23	2.591E+23
5.00E+01	2.555E+23	2.524E+23	2.572E+23	2.537E+23	2.506E+23	2.593E+23
6.00E+01	2.556E+23	2.524E+23	2.573E+23	2.538E+23	2.507E+23	2.593E+23
8.00E+01	2.557E+23	2.525E+23	2.574E+23	2.539E+23	2.507E+23	2.594E+23
1.00E+02	2.557E+23	2.525E+23	2.574E+23	2.539E+23	2.508E+23	2.594E+23
1.50E+02	2.557E+23	2.525E+23	2.574E+23	2.539E+23	2.508E+23	2.595E+23
2.00E+02	2.557E+23	2.525E+23	2.574E+23	2.539E+23	2.508E+23	2.595E+23
3.00E+02	2.557E+23	2.525E+23	2.574E+23	2.539E+23	2.508E+23	2.595E+23
4.00E+02	2.557E+23	2.525E+23	2.574E+23	2.539E+23	2.508E+23	2.595E+23
5.00E+02	2.557E+23	2.525E+23	2.574E+23	2.539E+23	2.508E+23	2.595E+23
6.00E+02	2.557E+23	2.525E+23	2.574E+23	2.539E+23	2.507E+23	2.594E+23
8.00E+02	2.557E+23	2.525E+23	2.574E+23	2.539E+23	2.507E+23	2.594E+23
1.00E+03	2.557E+23	2.525E+23	2.574E+23	2.539E+23	2.507E+23	2.594E+23
1.50E+03	2.557E+23	2.525E+23	2.573E+23	2.538E+23	2.507E+23	2.594E+23
2.00E+03	2.557E+23	2.525E+23	2.573E+23	2.538E+23	2.507E+23	2.594E+23
3.00E+03	2.557E+23	2.525E+23	2.573E+23	2.538E+23	2.507E+23	2.594E+23
4.00E+03	2.556E+23	2.524E+23	2.573E+23	2.538E+23	2.507E+23	2.594E+23
5.00E+03	2.557E+23	2.525E+23	2.574E+23	2.538E+23	2.507E+23	2.594E+23
6.00E+03	2.556E+23	2.524E+23	2.573E+23	2.538E+23	2.507E+23	2.594E+23
8.00E+03	2.556E+23	2.524E+23	2.573E+23	2.538E+23	2.507E+23	2.594E+23
1.00E+04	2.556E+23	2.524E+23	2.573E+23	2.538E+23	2.507E+23	2.594E+23
1.50E+04	2.556E+23	2.524E+23	2.573E+23	2.538E+23	2.507E+23	2.594E+23
2.00E+04	2.556E+23	2.524E+23	2.573E+23	2.538E+23	2.507E+23	2.593E+23
3.00E+04	2.556E+23	2.524E+23	2.573E+23	2.538E+23	2.507E+23	2.594E+23
4.00E+04	2.556E+23	2.524E+23	2.573E+23	2.538E+23	2.507E+23	2.593E+23
5.00E+04	2.556E+23	2.524E+23	2.573E+23	2.538E+23	2.507E+23	2.594E+23
6.00E+04	2.556E+23	2.524E+23	2.573E+23	2.538E+23	2.507E+23	2.594E+23
8.00E+04	2.556E+23	2.525E+23	2.573E+23	2.538E+23	2.507E+23	2.594E+23
1.00E+05	2.556E+23	2.524E+23	2.573E+23	2.538E+23	2.507E+23	2.594E+23

photon energy dependencies are reduced at intermediate incident photon energies because the Compton scattering process becomes the main type of photon interaction. In the high energy range, the variation of these parameters with the chemical composition again becomes important, and these parameters become almost independent of the photon energy because of the dominance of the pair-production process.

We can also conclude that the radiation shielding effectiveness of the cerrobend alloys investigated in this work will increase in the following order: Safe alloy > Bend alloy > Low 147 alloy > Low 136 alloy > Tru alloy > Cast alloy. The Safe alloy, Bend alloy, and Low 147 alloy have good radiation attenuation properties and hence absorb maximum amounts of gamma rays; therefore, they would be preferred as shielding materials against gamma radiation.

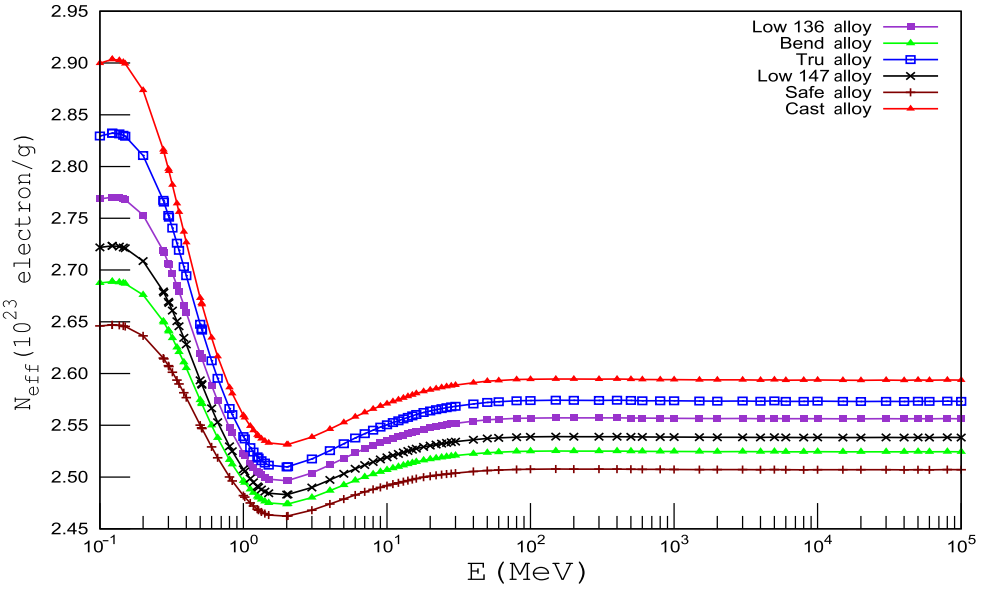

Fig. 15. The variation of the effective electron density of cerrobend alloys with incident photon energies.

However, the Low 136 alloy, Tru alloy, and Cast alloy demonstrate poor radiation attenuation properties.

Although the cerrobend alloys have seen large usage scale in radiotherapy and medical imaging, no further information is available on their μ_t, Z_{eff}, N_{eff}, HVL, and TVL values. To the best of our knowledge, the data presented are the first of their kind and have not been reported previously. This motivated us to undertake the present investigation. Moreover, the results of this present investigation are extremely important for radiation shield design in radiotherapy and medical imaging.

Conflicts of interest

We have no conflict of interest.

References

[1] I. Akkurt, Effective atomic and electron numbers of some steels at different energies, Ann. Nucl. Energy 36 (2009) 1702–1705.
[2] I. Akkurt, A.M. El-Khayatt, Effective atomic number and electron density of marble concrete, J. Radioanal. Nucl. Chem. 295 (2013) 633–638.
[3] I.M. Borchardtt, J.R. Pattersont, A.H. Beddoef, G.C. Sorellf, An investigation of photonuclear reactions in Cerrobend eutectic material with an 18 MV linac, Phys. Med. Biol. 36 (1991) 649–653.
[4] I.A. Brezovich, K.S. Sparks, J. Duan, A self-correcting method for improving the precision of beam blocks, J. Appl. Clin. Med. Phys. 2 (2001) 106–113.
[5] Y. Elmahroug, B. Tellili, C. Souga, Determination of total mass attenuation coefficients, effective atomic numbers and electron densities for different shielding materials, Ann. Nucl. Energy 75 (2015a) 268–274.
[6] Y. Elmahroug, B. Tellili, C. Souga, K. Manai, ParShield: a computer program for calculating attenuation parameters of the gamma rays and the fast neutrons, Ann. Nucl. Energy 76 (2015b) 94–99.
[7] Y. Elmahroug, B. Tellili, C. Souga, Determination of shielding parameters for different types of resins, Ann. Nucl. Energy 63 (2013) 619–623.
[8] S. Gowda, S. Krishnaveni, T. Yashoda, T.K. Umesh, R. Gowda, Photon mass attenuation coefficients, effective atomic numbers and electron densities of some thermoluminescent dosimetric compounds, Pramana J. Phys. 63 (2004) 529–541.
[9] G.J. Hine, The effective atomic numbers of materials for various gamma interactions, Phys. Rev. 85 (1952) 725–737.
[10] J.H. Hubbell, Review of photon interaction cross section data in the medical and biological context, Phys. Med. Biol. 44 (1999) R1.
[11] J.H. Hubbell, Photon mass attenuation and energy-absorption coefficients, Int. J. Appl. Radiat. Isot. 33 (1982) 1269–1290.
[12] O. Içelli, Z. Yalçina, M. Okutana, R. Boncukçuoğlub, A. Şen, The determination of the total mass attenuation coefficients and the effective atomic numbers for concentrated colemanite and Emet colemanite clay, Ann. Nucl. Energy 38 (2011) 2079–2085.
[13] P. Limkitjaroenporn, J. Kaewkhao, S. Asavavisithchai, Determination of mass attenuation coefficients and effective atomic numbers for Inconel 738 alloy for different energies obtained from Compton scattering, Ann. Nucl. Energy 53 (2013) 64–68.
[14] L. Ma, W. Chang, M. Lau-Chin, E.M. Tate, A.L. Boyer, Using static MLC fields to replace partial transmission cerrobend blocks in treatment planning of rectal carcinoma cases, Med. Dosim. 23 (1998) 264–266.
[15] S.R. Manohara, S.M. Hanagodimath, K.S. Thind, L. Gerward, On the effective atomic number and electron density: a comprehensive set of formulas for all types of materials and energies above 1 keV, Nucl. Instrum. Methods B 266 (2008) 3906–3912.
[16] Y. Mejaddem, I. Lax, A.K. Shamsuddin, Procedure for accurate fabrication of tissue compensators with high-density material, Phys. Med. Biol. 42 (1997) 415–421.
[17] G. Neuner, M.M. Mohiuddin, W.N. Vander, O. Goloubeva, J. Ha, C.X. Yu, W.F. Regine, High-dose spatially fractionated GRID radiation therapy (SFGRT): a comparison of treatment outcomes with Cerrobend vs. MLC SFGRT, Int. J. Radiat. Oncol. Biol. Phys. 82 (2012) 1642–1649.
[18] J.B. Wojcick, R. Yankelevich, B.L. Werner, D.E. Lasher, Technical Note: on Cerrobend shielding for 18–22 MeV electron beams, Nonlinearity 35 (2008) 4625–4629.